

Beam collimation with polycapillary x-ray optics for high contrast high resolution monochromatic imaging

Francisca R. Sugiro

Health Imaging Division, Eastman Kodak Company, Rochester, New York 14650

Danhong Li and C. A. MacDonald

Center for X-ray Optics, University at Albany, Albany, New York 12222

(Received 20 February 2004; revised 4 August 2004; accepted for publication 31 August 2004; published 19 November 2004)

Monochromatic imaging can provide better contrast and resolution than conventional broadband radiography. In broadband systems, low energy photons do not contribute to the image, but are merely absorbed, while high energy photons produce scattering that degrades the image. By tuning to the optimal energy, one can eliminate undesirable lower and higher energies. Monochromatization is achieved by diffraction from a single crystal. A crystal oriented to diffract at a particular energy, in this case the characteristic line energy, diffracts only those photons within a narrow range of angles. The resultant beam from a divergent source is nearly parallel, but not very intense. To increase the intensity, collimation was performed with polycapillary x-ray optics, which can collect radiation from a divergent source and redirect it into a quasi parallel beam. Contrast and resolution measurements were performed with diffracting crystals with both high and low angular acceptance. Testing was first done at 8 keV with an intense copper rotating anode x-ray source, then 17.5 keV measurements were made with a low power molybdenum source. At 8 keV, subject contrast was a factor of five higher than for the polychromatic case. At 17.5 keV, monochromatic contrast was two times greater than the conventional polychromatic contrast. The subject contrasts measured at both energies were in good agreement with theory. An additional factor of two increase in contrast, for a total gain of four, is expected at 17.5 keV from the removal of scatter. Scatter might be simply removed using an air gap, which does not degrade resolution with a parallel beam. © 2004 American Association of Physicists in Medicine. [DOI: 10.1118/1.1809779]

Key words: polycapillary x-ray optics, monochromatic imaging, subject contrast, angular resolution

I. INTRODUCTION

Mammographic imaging has proven to be the most effective way to detect and diagnose early stages of tumor in breasts, which is vital to reducing mortality. Because early diagnosis is the key to reducing mortality, it is essential to provide the clearest possible image and minimize the rate of false readings.

Conventional imaging has been hampered by the wide spectrum of radiation emitted by x-ray tubes. Soft x rays only increase patient dosage. On the other end of the spectrum, high energies produce less subject contrast and give rise to scattered radiation. This reduces visibility of structures within the tissues. Monochromatic beams give maximum intensity at the optimum energy¹ and increase the difference between linear attenuation coefficients of different tissues compared to the usual average values over a wide energy range.^{2,3} Contrast between carcinoma and breast parenchyma that is usually indistinguishable due to small differences in linear attenuation coefficient can be significantly enhanced by the use of monochromatic beams.⁴⁻⁷ Monochromatizing the beam would also, by removing the soft x rays, reduce patient dose.

A major problem with monochromatic imaging, and the reason it has been traditionally limited to research sources

such as synchrotrons, which are expensive for mammographic screening, is that of obtaining sufficient beam intensity.

Monochromatization is achieved by diffracting an x-ray beam from a crystal. Diffraction only occurs for that part of the x-ray beam that is incident at the correct angle for the selected energy according to Bragg's law⁸

$$\lambda = \frac{hc}{E} = 2d \sin \theta, \quad (1)$$

where d is the crystal plane spacing, θ is the angle between the x-ray beam and the crystal surface, and E is the x-ray energy. The diffracted intensity from divergent sources is low because only a small fraction of the incident beam is at the right energy and the right angle. However, high diffracted beam intensity can be achieved by first collimating the divergent beam from conventional sources by using polycapillary optics.^{9,10} A collimating optic collects a large solid angle from an x-ray source and redirects the photons into a parallel beam directed towards the crystal, thereby making more efficient use of the x-ray source.

Polycapillary collimating optics are bundles of hollow glass tubes shaped to collect and redirect the x-ray emission into a parallel beam. These optics guide x rays in a manner

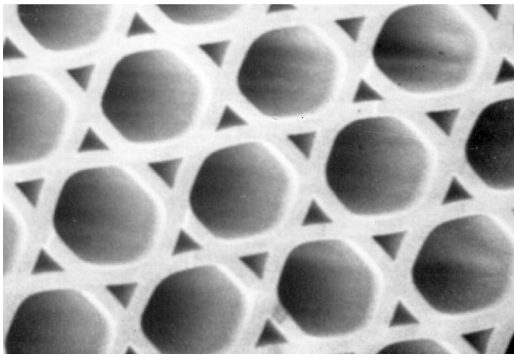


FIG. 1. Cross-sectional SEM photograph of a polycapillary fiber with 10 μm diameter channels.

analogous to the way fiber optics guide light.^{11,12} X rays are deflected by total external reflection from the capillary surfaces at very small angles.¹³ The reflection of x rays, which bounces them down the length of the capillary, is governed by the critical angle, which is energy dependent. For borosilicate glass, the critical angle is approximately

$$\theta_c \approx \frac{30}{E(\text{keV})} \text{mrad}. \quad (2)$$

For 8 keV photons, the critical angle is approximately 4 mrad or 0.23° .

X rays can be transmitted down a curved fiber as long as the fiber is small enough and bent gently enough to keep the angles of incidence less than the critical angle. The requirement that the incident angles remain less than the critical angle necessitates the use of very small tube diameters. However, mechanical limitations prohibit the manufacture of the capillary fibers with outer diameters smaller than 300 μm . For this reason, polycapillary fibers, as shown in Fig. 1, are employed.

Thousands of these fibers are strung through lithographically produced metal grids to produce a multi-fiber optic, which is shaped into a collimating optic, shown in Fig. 2. In addition to making more efficient use of the source to provide higher diffracted intensity, the resultant parallel beam would eliminate the variations in resolution from the differ-



FIG. 2. Multifiber collimating lens with 20×20 mm output, 8.07×8.07 mm input, focal length (optimal distance to source) of 250 mm, length 127 mm, and transmission efficiency of 37% at 17.5 keV.

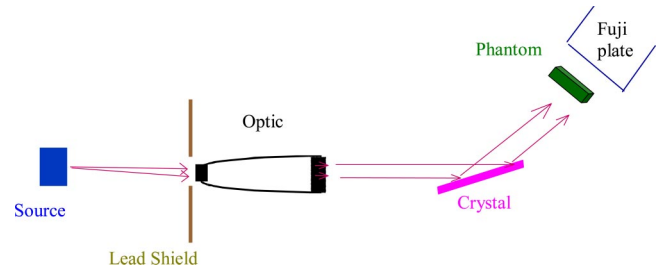


FIG. 3. Monochromatic imaging setup.

ent apparent source sizes viewed from different parts of the x-ray field when a conventional line source is used. Image distortion arising from the different magnification of the objects on the entry and exit side of the patient would also be eliminated. Importantly, scatter could be virtually eliminated by the larger air gap made possible by the more parallel beam. A parallel beam would also relax geometrical constraints that have affected system design. After collimation, changes in optic-to-patient distances would not affect magnification or resolution. In addition, because the beam would pass through the polycapillary optic/crystal combination before reaching the patient, the patient would not be exposed to radiation lost in the process of monochromatizing the beam and so the dose would not increase (and would actually be reduced due to the resultant higher subject contrast).

Diffracted beam intensity depends on the angular divergence of the incident beam, hence the need for collimation, and also on the angular acceptance bandwidth of the crystal. The choice of crystal is a trade-off between intensity and resolution. Crystals with large bandwidth accept a larger fraction of the incident beam, but the higher angular divergence results in larger geometrical blur. Small bandwidth crystals such as silicon (0.02 mrad) give high resolution but low intensity. On the other hand, large bandwidth crystals such as graphite (42.5 mrad) yield good intensity, but insufficient resolution. Mica, which has a bandwidth of 0.4–0.6 mrad, is a good middle ground between silicon and graphite.

A collimating optic/crystal combination is essential to create an x-ray beam with intensity sufficient for rapid imaging. Both the optic and crystal when used alone are problematic. An essential difficulty in using a collimating optic by itself (aside from the lack of monochromaticity) lies in the output divergence of each polycapillary channel. The output diver-

TABLE I. Optic parameters. The second optic has a shorter focal distance appropriate for use with a compact source.

	Optic A076-H9	Optic 1201-01
Length (mm)	127	40.8
Input Area (mm^2)	$8.07 \times 8.07 = 65.12$	$\pi (2.84/2)^2 = 6.33$
Source to Optic Distance (mm)	250	48.4
Input Capture Angle	64.6 mrad	116.9 mrad
Transmission	40% at 8 keV	6% at 17.5 keV
Output Area (mm^2)	$10 \times 10 = 100$	$\pi (4.0/2)^2 = 12.57$
Output Angular Divergence	4 mrad at 8 keV	2.4 mrad at 17.5 keV

TABLE II. Crystals used for monochromatizing the beam, with their orientation (which set of crystal planes are parallel to the surface) and the spacing, d , between the atomic planes (Refs. 22 and 23). Equation (1) is used to compute the Bragg angle θ which is different for different wavelengths (energies). For silicon (and graphite) the Bragg angle is computed for the 4th (2nd) order diffracted beam, since the theoretical intensity from the lower order diffractions is zero due to destructive interference (Ref. 24). The mica was supplied by XOS, Inc. and Ted Pella, Inc. and the pyrolytic graphite, graded ZYH, by Advanced Ceramics Corporation.

Crystal	Orientation	Plane spacing, d , nm	Bragg angle		
			Cu $K\alpha$ (8 keV)	Mo $K\alpha$ (17.4 keV)	Mo $K\beta$ (19.5 keV)
Silicon (Si)	(100)	0.137 (400)	34.44°	15.25°	13.55°
Mica (muscovite, K ₂ O 3Al ₂ O ₃ 6SiO ₂ 2H ₂ O)	(0010)	0.199	22.93°	10.33°	9.19°
Graphite (C)	(001)	0.168 (002)	13.36°	6.11°	5.45°

gence of the optic is approximately $1.5 \cdot \theta c$. For a 50 mm thick breast tissue sample, the geometrical blur at 20 keV would be 100 μm , or a resolution of 5 line-pairs/mm. This is insufficient resolution for imaging; therefore, a diffracting crystal must be incorporated with the optic to reduce angular divergence. The major problem in using a crystal alone to monochromatize a conventional source is obtaining sufficient beam intensity.

Since the optic/crystal technology could be applied to conventional x-ray sources in mammographic units, it could be used in low-cost screening systems. Monochromatizing a conventional x-ray source would allow routine screening mammography to take advantage of the higher contrast previously only available with synchrotron and other research sources. The availability of a parallel monochromatic source will also allow the use of other techniques such as refractive index contrast imaging using conventional sources.^{14,15}

II. METHODS AND ANALYSES

The basic setup of the measurements employing an x-ray source, an optic, a crystal, a phantom and a Fuji plate detector is shown in Fig. 3. The first measurements used a high intensity Rigaku copper rotating anode source to produce an 8 keV beam. Later a low power (20 W) molybdenum 5011 Ultrabright XRM series Oxford source was used for measurements at 17.5 keV. Two different optics were employed. Geometrical and performance parameters for the optics are listed in Table I. The primary difference between the optics is that optic A076 H9 was designed for the rotating anode source, which has a longer distance between the x-ray anode

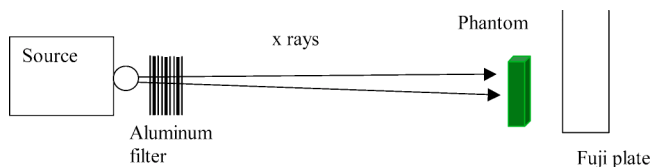


FIG. 4. Experimental setup for polychromatic imaging, without an optic or crystal. The 5.56 mm thick aluminum filters were placed before the phantom to avoid over-exposing the Fuji image plate. The exposure time for this source with the aluminum filter was about 30 s, which was about the minimum required for this source to come up to full voltage (this source is normally used in continuous, not pulsed, operation).

and the vacuum window, so the minimum source to optic distance is larger. The second optic was designed for a more compact source and has a smaller input focal distance, which gives it a larger capture angle despite its smaller size.

The detector was a computed radiography plate, Bio-Imaging Analyzer BAS-1800 manufactured by Fuji Photo Film Co., Ltd. The phantoms were a Rose block, Lucite blocks with holes of varying depth, and polypropylene and polyvinyl chloride step phantoms. Contrast of these phantoms was measured with a polycapillary collimating optic, without the optic, and with an optic/crystal combination. Silicon, mica, and graphite crystals were used for monochromatization. The crystals are listed in Table II. The primary difference between the crystals is their acceptance bandwidth, which range from very narrow for silicon to very broad for graphite.

Using this setup, the phantom contrast was measured and compared to theoretical values. Finally, the spatial resolution of the system was tested with a knife-edge and compared to theoretical values.

A. Contrast at 8 keV

Testing was begun with a copper rotating anode at 8 keV, because it was the most intense source available. X rays at 8 keV would be absorbed by a 50 mm thick patient, so the

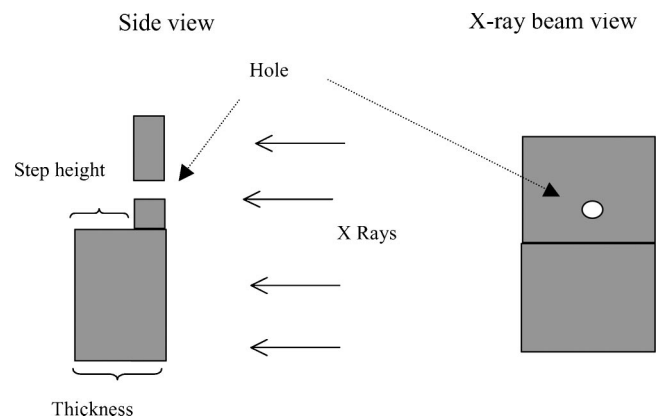


FIG. 5. The construction of the 8 keV step phantoms. In the beam view the x-ray beam is coming straight out of the paper.

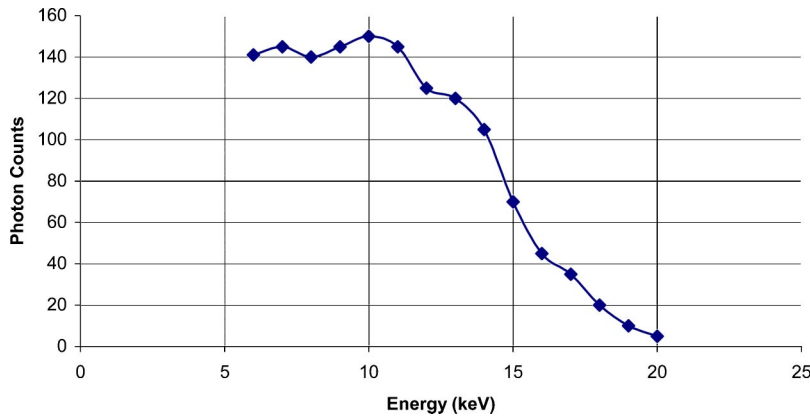


FIG. 6. Copper rotating anode spectrum taken with a NaI detector through a 5.65 mm aluminum filter and a small pinhole.

source could only be used for preliminary testing. Mammographic imaging would be at higher energies. The setup for monochromatic imaging and for polychromatic, conventional imaging are shown in Figs. 3 and 4, respectively.

The primary benefit of the monochromatization is increased image contrast. Contrast was defined as the logarithmic expression

$$C = \ln\left(\frac{I_1}{I_2}\right), \tag{3}$$

where I_1 is the intensity through the area of interest, and I_2 is the adjacent intensity. A phantom to be used at 8 keV has to be relatively thin, about 1.5–15.5 mm. The phantoms were made of polypropylene plastic (recyclable plastic container type {5}) and polyvinyl chloride plastic (container type {3}). Because the useable phantoms are quite thin and the beam from the small test optics was quite narrow, less than 1 cm², the phantoms were too small to create significant scatter, and the theoretical contrast was taken as the ideal contrast without any reduction for scatter fraction.

The construction of the phantom is shown in Fig. 5. The step-height is the difference between the thicknesses of the upper and lower part. A hole was pierced in the plastic to

calibrate the direct beam gray scale for different images. Phantom images were taken without the optic (polychromatic, conventional) and with optic/crystal combination (monochromatic).

The theoretical contrast for polypropylene plastic (C₃H₆, mass attenuation coefficient μ/ρ of 3.67 and density ρ of 0.9 g/cm³) was calculated from Eq. (3) using attenuation values available in published tables.¹⁶ For the polychromatic case, the transmission was binned for each energy from 7 to 19 keV with a bin size of 1 keV. Then all 13 bins were weighted and averaged according to the experimental copper spectrum shown in Fig. 6. Contrast was also compared between the polypropylene and polyvinyl chloride, C₂H₃Cl, with μ/ρ of 62.76 and ρ of 1.4 g/cm³ using the mass absorption coefficient given in the NIST database.¹⁷

To confirm the contrast enhancement was solely due to monochromatizing and not to beam collimation, measurements were done with the optic alone, without the crystal and were compared to measurements without the collimating optic.

B. Contrast at 17.5 keV

Mammographic imaging applications should be performed at about 20 keV. A molybdenum tube was chosen

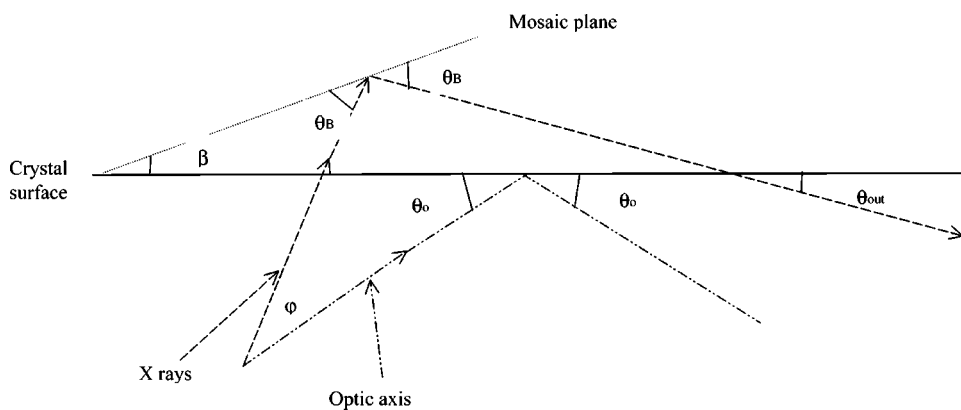


FIG. 7. Output of the x-rays off the crystal in two dimensions. The angle between the surface and the optic axis is set to θ_o . The angle of a particular plane to the crystal surface is β . The angle of the x-ray to the optic axis is φ . The angle of the x-ray to the plane is then $\theta_B = \varphi + \theta_o - \beta$. The angle of the reflected x-ray to the crystal surface is $\theta_{out} = \theta_o + \varphi - 2\beta = \theta_o + \Delta\theta$.

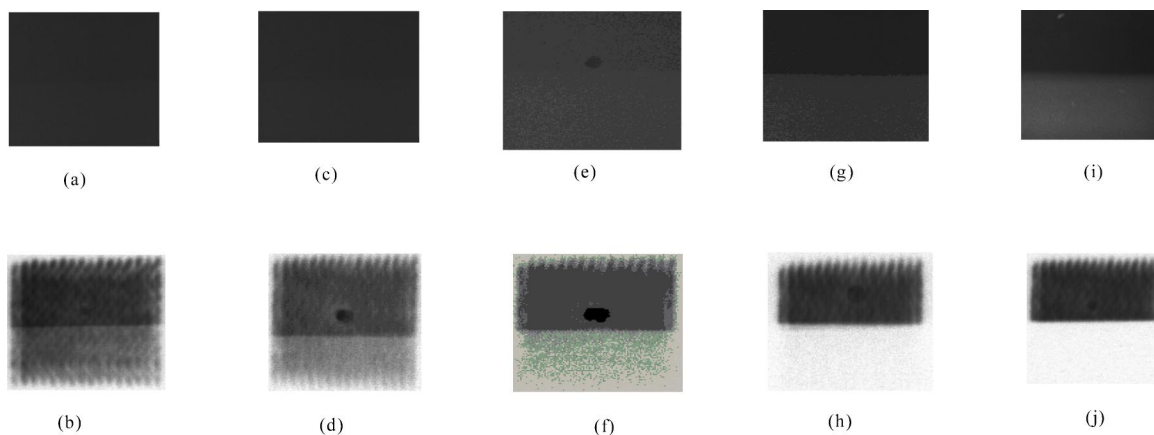


FIG. 8. Image plate data from five different polypropylene step phantoms. The top row was taken without the optic (conventional), the bottom row was taken with a monochromatic beam. Columns a/b is the phantom with a step height of 1.5 mm, columns c/d with 2.0 mm, columns e/f with 6.6 mm, columns g/h with 10.6 mm, and columns i/j with 15.5 mm. Notice that contrast is already visible in the monochromatic case even for the lowest step height.

because the $K\alpha$ and $K\beta$ peaks are at 17.5 and 19.5 keV. The molybdenum source with tube voltage of 25 kV was used to measure contrast in 45 mm thick Lucite Rose phantoms with different hole depths. The holes were 3 mm in diameter. Contrast at each depth without the optic was compared with the contrast using the optic and crystal. The theoretical contrast for the polychromatic case was computed as before but now for the range of 8–25 keV. Although the phantoms are thicker than at 8 keV the demonstration optic output for these measurements was very small, less than 0.1 cm^2 , so the phantoms were still too small to create scatter. Again the theoretical contrast was taken as the ideal contrast without any reduction for scatter fraction.

C. Resolution at 8 keV

The motivation for examining resolution in the system is that the angular divergence of the x-ray beam causes blurring in the image of small features at the entrance side of a thick phantom. Because the output beam of the optic is not completely parallel, the resolution is affected; therefore, the angular divergence must be controlled. The output divergence is an important parameter especially for low energy x rays

because the critical angle and thus the divergence of the optic at lower energy is greater than at higher energy. High resolution is needed at relatively low energy for mammography compared to other radiographic applications. Exit angle divergences from the capillary optics were measured by rotating a high quality crystal in the beam and measuring the angular width of the diffracted peak. Imaging measurements were then done with a variety of crystals. Each of these crystals was tuned to the Bragg angle for the copper $K\alpha$ peak.

To measure the resolution of the system, a knife-edge was placed after the monochromatic parallel beam, taking the place of the contrast phantom in Fig. 4, in between the crystal and the detector. An image plate was placed 300 mm from the knife-edge to achieve a measurement resolution of 0.17 mrad with the $50 \mu\text{m}$ pixels of the Fuji radiography plate detector. For a perfect crystal and parallel monochromatic input beam, with a perfect detector, the knife-edge image would be ideally sharp.

To predict the actual resolution, a calculation was developed. Differentiating Eq. (2) gives the relation between angle and energy spreads, $K\alpha$

TABLE III. Comparison of contrast for step phantoms using 8 keV monochromatic beams obtained with silicon, mica, and graphite crystals to the polychromatic contrast of conventional imaging, taken without crystals or the optic. The monochromatic contrast is independent of the crystal used, because even the widest crystal angular bandwidth gives an energy spread of only 1.4 keV. The polychromatic contrast is independent of whether or not an optic is used or the optic to phantom distance. Collimation does not affect the contrast.

Step-height (mm)	Contrast							
	Polychromatic				Monochromatic			
	Data		Theory	Data			Theory	
no optic	optic 0 cm	Silicon		Mica	Graphite			
1.5	0.2 ± 0.1	0.1 ± 0.2	0.2 ± 0.2	0.2	0.6 ± 0.4	0.7 ± 0.1	0.7 ± 0.3	0.6
2.0	0.2 ± 0.1	0.4 ± 0.3	0.4 ± 0.2	0.2	0.7 ± 0.3	0.9 ± 0.2	1.0 ± 0.2	0.7
6.6	0.4 ± 0.1	0.5 ± 0.1	0.5 ± 0.2	0.4	2.2 ± 0.5	1.8 ± 0.3	2.1 ± 0.2	2.2
10.6	0.8 ± 0.1	0.8 ± 0.1	0.8 ± 0.2	0.8	4.3 ± 0.5	3.8 ± 0.2	4.2 ± 0.3	3.8
15.5	1.2 ± 0.1	1.3 ± 0.2	1.1 ± 0.3	1.2	5.3 ± 0.4	5.2 ± 0.2	5.1 ± 0.5	5.2

TABLE IV. Contrast enhancement, monochromatic contrast divided by the polychromatic contrast, for the step phantoms at 8 keV using the silicon crystal.

Step-height (mm)	Contrast ratio	
	Data	Theory
1.5	3.0±2.6	3.0
2.0	4.1±2.5	3.5
6.6	5.4±2.5	5.7
10.6	5.3±1.1	4.8
15.5	4.4±0.6	4.3

$$\Delta\theta \equiv \tan \theta_o \frac{\Delta E}{E}. \tag{4}$$

This implies that the 4 eV energy width of the $K\alpha_2$ emission line at 8027.83 eV produces an angular spread of $\sigma_E = 0.34$ mrad.^{18,19}

Combining the effects of the crystal, optic divergence, and energy spread, the angular distribution of intensity off the crystal should be roughly given by

$$I(\Delta\theta) = \int \int I(\varphi)I(E(\beta))p(\beta)\delta(\Delta\theta - \varphi + 2\beta)d\varphi dE, \tag{5}$$

where $\Delta\theta$ is the deviation of the output angle from the normal Bragg angle, $I(\varphi)$ is the angular distribution from the optic, assumed to be a Gaussian of width σ_{optic} , $I(E)$ is the spectral distribution of the $K\alpha_2$ line, also assumed Gaussian, of width $\sigma_{K\alpha} = 4$ eV. Figure 7 shows the relationship between the different angles. The relationship between the angles and the energy from Bragg’s law is

$$E(\beta) = \frac{hc}{2d \sin \theta_B} = \frac{hc}{2d \sin(\theta_o + \varphi - \beta)} \approx E_{K\alpha} \left(1 - \frac{(\varphi - \beta)}{\tan \theta_o} \right). \tag{6}$$

The probability distribution $p(\beta)$ of planes at an angle β from the surface of the crystal is assumed to be Gaussian of width α , where α is the crystal bandwidth.

Making the appropriate substitutions, the integral in Eq. (5) becomes

$$I(\Delta\theta) \approx \frac{1}{\pi\sigma_{\text{optic}}\sigma_E} \int \exp\left[-\frac{\varphi^2}{\sigma_{\text{optic}}^2}\right] \exp\left[-\frac{(\varphi + \Delta\theta)^2}{4\sigma_E^2}\right] \times \exp\left[-\frac{(\varphi - \Delta\theta)^2}{4\alpha^2}\right] d\varphi. \tag{7}$$

Solving the integral analytically

$$I(\Delta\theta) = C \exp\left[-\frac{\Delta\theta^2}{\sigma^2}\right], \tag{8}$$

and the output width is

TABLE V. Contrast between polypropylene and polyvinyl chloride plastics were compared for the 8 keV monochromatic and polychromatic beams.

		Contrast		Contrast ratio	
		Data	Theory	Data	Theory
Polychromatic		0.5±0.1	0.5		
Monochromatic	silicon	3.0±0.3	2.9	6.4±2.2	6.0
	mica	3.0±0.4		6.4±2.5	
	graphite	2.6±0.2		5.5±1.9	

$$\sigma = \sqrt{\frac{4\sigma_E^2 \cdot \alpha^2 + \sigma_E^2 \cdot \sigma_{\text{optic}}^2 + \sigma_{\text{optic}}^2 \cdot \alpha^2}{\alpha^2 + \sigma_{\text{optic}}^2 + \sigma_E^2}}. \tag{9}$$

Equation (9) is used for calculating the theoretical angular resolution. A more detailed three-dimensional calculation is underway.²⁰

D. Resolution at 17.5 and 19.5 keV

Mammography is typically performed with a molybdenum x-ray source. The resolutions measured at 8 keV were very promising. Therefore, this study was continued for the $K\alpha$ and $K\beta$ peaks of molybdenum. These measurements were performed with optic 1201-01 with a knife-edge to detector distance of 400 mm.

III. RESULTS AND DISCUSSIONS

A. Contrast at 8 keV

Monochromatic and polychromatic images for the five step height phantoms are shown in Fig. 8. An optic to phantom distance of 43 cm was chosen because at that distance the fiber structure is sufficiently blurred not to be observable in the images. This is further discussed in the resolution section. The contrast data and calculation results are shown in Table III. The contrast is much higher for the monochromatic case, in agreement with the theoretical calculations. The different bandwidth crystals yielded similar contrast values. This is because the energy width given by Eq. (4) for even the widest bandwidth crystal, graphite, is only 1.4 keV. The resulting contrast enhancement, the monochromatic contrast over the polychromatic value, shown in Table IV, is about fivefold.

TABLE VI. Contrast at 17.5 keV with 45 mm lucite phantom.

Depth (mm)	Contrast					
	Polychromatic		Monochromatic		Ratio	
	Data	Theory	Data	Theory	Data	Theory
35	1.3±0.1	1.3	2.4±0.3	2.9	1.8±0.6	2.2
30	1.2±0.1	1.0	2.1±0.3	2.5	1.8±0.4	2.5
20	0.8±0.1	0.6	1.4±0.4	1.7	2.2±0.9	2.8
15	0.4±0.1	0.5	0.7±0.4	0.8	1.5±0.9	1.6

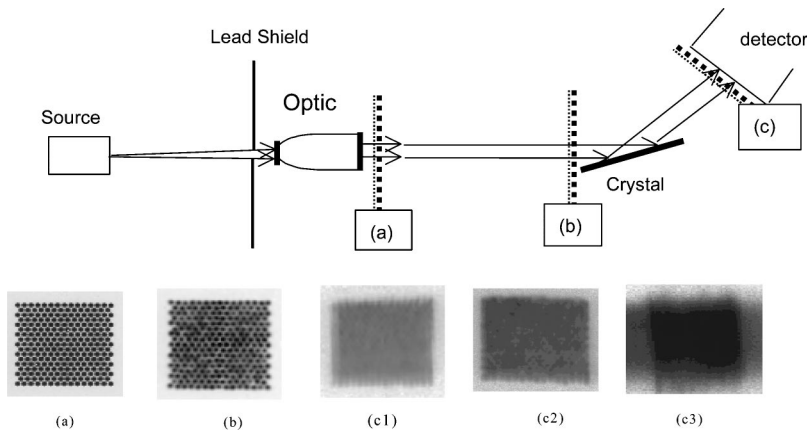


FIG. 9. Set-up for monochromatic imaging. The double dotted lines correspond to the image locations (a)–(c) displayed below the setup. The fiber structure of the optic is clearly visible in (a). Location of (b) is 17 cm after the optic. The divergence has blurred the fiber structure. Post crystal images are labeled for silicon (c1), for mica (c2), and for graphite (c3). Aluminum filters of varied thickness were used for (a) through (c) except for imaging with silicon and mica crystals.

To verify that collimation alone was not affecting the contrast without the monochromatization, contrast measurements were performed without the crystal, with the phantom close to the collimating optic and 43 cm away from the optic. That distance was selected to be equal to the total distance from optic to crystal to the detector for the monochromatic case. As shown in Table III, in all cases, the contrasts were identical within the experimental error to the no optic case. Collimation did not affect the contrast.

In mammography, tissue typology must be distinguished on the image. Therefore, different types of plastic with the same thickness of 1.5 mm, but different composition and density were compared. Table V shows the contrast between the polypropylene and polyvinylchloride for the polychromatic case and for the monochromatic case with the three different diffracting crystals. The contrast ratio is six, which was very promising, so work was continued at higher energies.

B. Contrast at 17.5 keV

Contrast images of the 45 mm poly(methylmethacrylate) (PMMA) phantom with different hole depths were measured with a silicon crystal rotated to diffract the molybdenum $K\alpha_2$ line. The contrast values are summarized in Table VI. Contrast enhancement of more than two was found, which agrees well with theoretical calculations.

Although the phantoms employed in this experiment were too small to create significant scatter fractions, larger beams in a practical clinical system would generate scatter. This would reduce the contrast for both the polychromatic and monochromatic cases. However, the parallel beam resulting from monochromatization simplifies scatter removal. As has been previously demonstrated using polycapillary optics as anti-scatter grids, efficient removal of scatter increases the system contrast by a factor of two.²¹ This is independent of the increase in subject contrast due to the monochromatization. Therefore the combined effect of monochromatization and efficient scatter removal would be a factor of four increase in contrast compared to the conventional case.

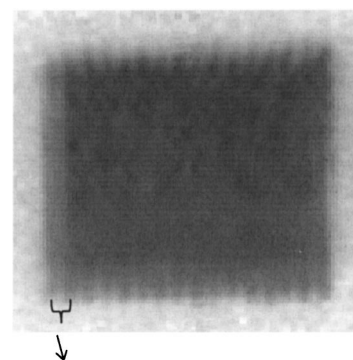
Production of images even with a very low power, 20 W source indicates that monochromatization at mammographic energies with conventional sources is feasible.

C. Resolution at 8 keV

The placement of the crystal for measuring the divergence and for monochromatic imaging is the same, and is shown in Fig. 9. The output divergence of the optic, in addition to affecting resolution, blurred the effect of the fiber structures of the optic. Images of the x-ray field immediately after the optic, 17 cm from the optic, and after the crystals are shown in Fig. 9. After the crystal, the fiber structure is much less apparent.

Since the angular bandwidth of graphite is wide, the image from the graphite crystal in Fig. 9 was wide and blurred. The image of the optic after the silicon crystal is narrow, but had an extra “shadow” on the left hand side expanded in Fig. 10. The width of this shadow was 1.12 mm. The shadow is due to the separation of the copper $K\alpha_1$ and $K\alpha_2$ lines, which is about 20 eV, corresponding to an angle of 3.7 mrad or a distance on the image plate of 0.5 mm. The additional blur of 0.6 mm was due to the optic divergence of 4 mrad, at an optic to detector distance of 150 mm.

Because the optic has a slightly divergent output, and each crystal has a finite acceptance width, the crystals can be rocked slightly off the Bragg angle and still diffract some beam. The rocking curves for the $K\alpha$ copper line measured with each of the three crystals are shown in Fig. 11. For the



The extra shadow of width 1.12 mm.

FIG. 10. A magnified picture after the silicon crystal clearly indicates the extra shadow of the $K\alpha$ doublet separation.

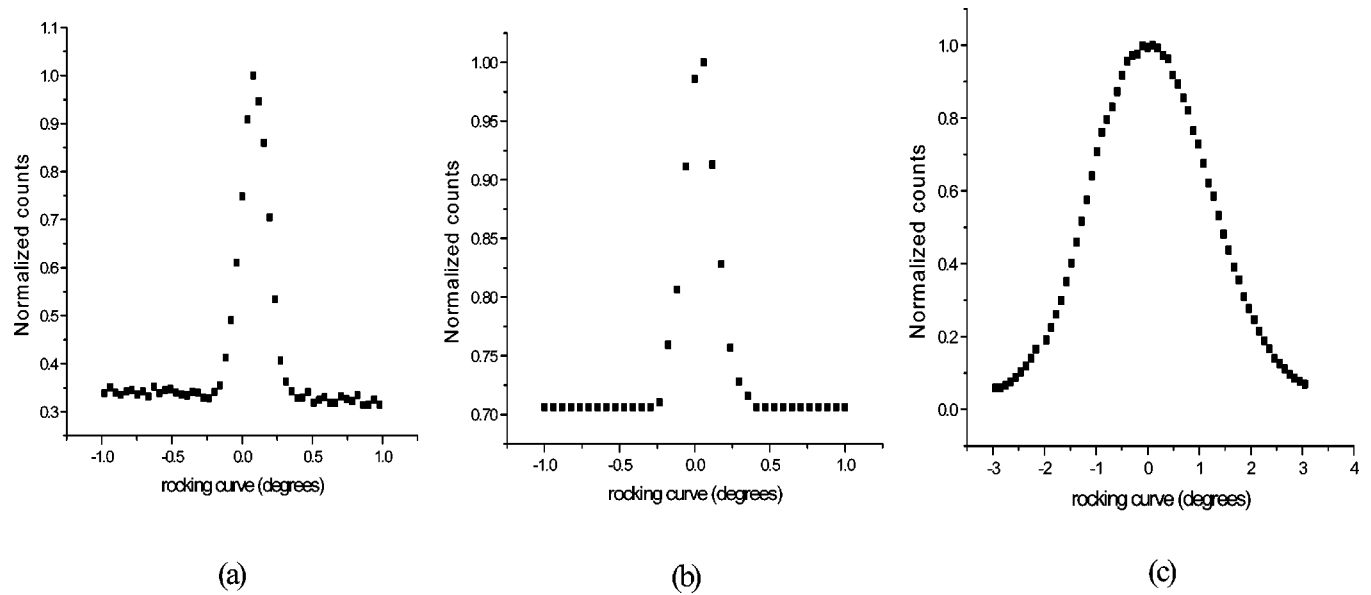


FIG. 11. Rocking curves of three crystals: Silicon (a) with full width at half maximum (FWHM) 4.0 mrad, mica (b) with FWHM 4.4 mrad, and graphite (c) with FWHM 42.5 mrad. Note the change in scale for graphite rocking curve.

TABLE VII. Rocking curves and resolution measurements using three different crystals. The rocking curve widths are due to the combined effects of the angular bandwidth of the crystal and the 4 mrad output divergence of the optic. The effect of the detector has been subtracted. The angular resolution calculations are given by Eq. (9). The energy width for graphite is taken to include the whole $K\alpha$ doublet.

Crystals	Manufacturer specification for α (mrad)	Measured rocking curve width (mrad) at Cu $K\alpha_2$	Measured angular width of knife-edge image (mrad)	Theory angular width, σ (mrad)
Silicon	0.02	4.0 ± 0.1	0.51 ± 0.20	0.57
Mica	0.4–0.6	4.4 ± 0.2	0.76 ± 0.20	0.53–0.69
Graphite	35–87	42.5 ± 1.1	6.5 ± 0.5	4.5

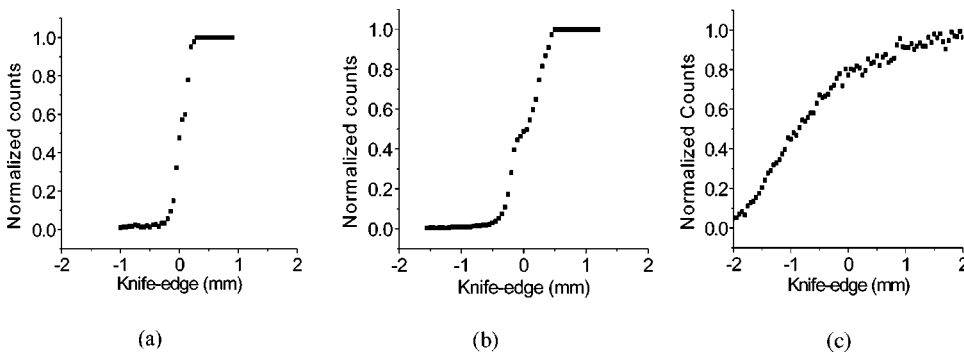


FIG. 12. Knife-edge resolution profiles obtained with silicon (a), mica (b) and graphite (c) crystals. The edge shows a double step for silicon and mica due to the $K\alpha$ doublet separation.

TABLE VIII. The angular resolution obtained for the molybdenum $K\alpha_2$ and $K\beta$ peaks. The first column is the measured angular width of the knife edge image, after subtracting the detector contribution. The theory is computed from Eq. (9). The resolution is computed given the theoretical angular width, for a 50 mm thick patient with an ideal detector.

Crystal	at Mo $K\alpha_2$			at Mo $K\beta$		
	Angular width (mrad)		Resolution (lp/mm)	Angular width (mrad)		Resolution (lp/mm)
	Measured	Theory		Measured	Theory	
Silicon	0.17 ± 0.02	0.12	83	0.25 ± 0.06	0.10	100
Mica	0.59 ± 0.06	0.40–0.59	20	0.77 ± 0.17	0.40–0.58	20
Graphite	2.42 ± 0.21	2.36	4	2.74 ± 0.13	2.28	4

narrowest bandwidth crystal, silicon, the entire rocking curve width is due to the optic divergence, so that width is taken as σ_{optic} . For mica, the width is a combination of the divergence and the crystal width. For graphite, the crystal dominates. The widths of the curves are given in Table VII.

With the crystals returned to the Bragg angle, knife edge images were made. The intensity profiles obtained from the images made with silicon, mica, and graphite crystals are shown in Fig. 12. The derivative of the intensity profile was calculated for the step corresponding to the $K\alpha_2$ emission line. The experimental angular resolutions were taken as the widths of the derivatives of the knife-edge profiles. The angular width contributed by the detector was subtracted in quadrature from the measured value

$$\sigma = \sqrt{\sigma_{\text{measured}}^2 - (0.17 \text{ mrad})^2}. \quad (10)$$

The results are shown in Table VII. The values agree fairly well with the calculated resolutions from Eq. (9), which suggested that it would be promising to progress to the molybdenum measurements.

D. Resolution at 17.5 and 19.5 keV

The expected resolution at the molybdenum $K\alpha$ and $K\beta$ peaks can be calculated using the same procedure as at 8 keV. Assuming the individual $K\alpha$ and $K\beta$ peaks have a width of 7.7 eV,¹⁸ the theoretical resolution was computed using Eq. (9). The rocking curve width for optic 1201 measured with the silicon crystal was 2.36 mrad at the 17.5 keV energy of the $K\alpha$ peak, so that value were taken as the output divergence of the optic. At the $K\beta$ peak at 19.5 keV it was 2.28 mrad. The optic divergence is energy dependent because it is limited by twice the critical angle. The experimental and theoretical resolutions using silicon, mica, and graphite are given in Table VIII. The data agreed with the calculated values. The last column in the table shows the corresponding angular resolution for a 50 mm thick phantom in lp/mm. At mammographic energies, monochromatic imaging shows a resolution of 20 lp/mm or better with silicon and mica crystals.

IV. CONCLUSION

These measurements have shown promise in producing high contrast high resolution monochromatic images with a conventional divergent source. A conventional divergent x-ray source needs collimating optics to produce high enough intensity for use in monochromatic x-ray imaging. Contrast of step height phantoms was enhanced by five at 8 keV relative to the conventional polychromatic case. Contrast enhancement for a phantom of varying composition was six. All contrast measurements were in good agreement with theory. The measured angular resolution with a silicon crystal was 0.5 mrad at 8 keV, in agreement with the described calculation technique. The contrast improvement factor of five at 8 keV and two at 17.5 keV suggests that monochromatic imaging may be promising when used in clinical settings with conventional sources. The resolution at 17.5 and 19.5 keV shows 20 lp/mm with mica crystals. Mica crystals are a good middle ground between high resolution versus high intensity. These results at 8, 17.5, and 19.5 keV suggest the technique could be applicable using a variety of energies where imaging is practiced in clinical settings.

ACKNOWLEDGMENTS

The authors wish to acknowledge X-ray Optical Systems, Inc. for supplying the optics and mica crystals. This project was supported by the Department of Defense Breast Cancer Research Grant No. DAMD17-99-1-9316 and DAMD 170210517.

¹R. Fahrig and M. J. Yaffe, "Optimization of spectral shape in digital mammography, dependence on anode material, breast thickness, and lesion type," *Med. Phys.* **21**, 1473–1481 (1994).

²J. M. Boone and J. A. Seibert, "A comparison of mono- and polyenergetic x-ray beam performance for radiographic and fluoroscopic imaging," *Med. Phys.* **21**, 1853–1863 (1994).

³R. J. Jennings, P. W. Quinn, R. M. Gagne, and T. R. Fewell, "Evaluation of x-ray sources for mammography," *Phys. Med. Imaging, SPIE* **1896**, 259–269 (1993).

⁴M. Gambaccini, A. Tuffanelli, A. Taibi, A. Fantini, and A. Del Guerra, "Bragg-diffraction-based quasi-monochromatic source for mammography using mosaic crystals," *Proc SPIE Int. Soc. Opt. Eng.* **3770**, 174 (1999).

⁵R. Fairchild, H. L. Atkins, E. Lebowitz, and D. Greenberg, "Investigation of I-125 as an isotopic source for mammography," *Invest. Radiol.* **10**, 511–518 (1975).

⁶F. E. Carroll *et al.*, "Attenuation of monochromatic x rays by normal and

- abnormal breast tissues," *Invest. Radiol.* **29**, 266–272 (1994).
- ⁷R. E. Johnston *et al.*, "Mammographic phantom studies with synchrotron radiation," *Radiology* **200**, 659–663 (1996).
- ⁸B. D. Cullity, *Elements of X-ray Diffraction*, 2nd ed. (Addison-Wesley, Reading, 1978).
- ⁹C. A. MacDonald, S. M. Owens, and W. M. Gibson, "Polycapillary x-ray optics for microdiffraction," *J. Appl. Crystallogr.* **32**, 160–167 (1999).
- ¹⁰F. A. Hofmann, W. M. Gibson, C. A. MacDonald, D. A. Carter, J. X. Ho, and J. R. Ruble, "Polycapillary optic-source combination for protein crystallography," *J. Appl. Crystallogr.* **34**, 330–335 (2001).
- ¹¹C. A. MacDonald, "Applications and measurements of polycapillary x-ray optics," *J. X-Ray Sci. Technol.* **6**, 32–47 (1996).
- ¹²C. A. MacDonald and W. M. Gibson, "Polycapillary and multichannel plate x-ray optics," in *Handbook of Optics*, edited by M. Bass (McGraw-Hill, New York, 2000), Chap. 30, Vol. III, pp. 30.1–30.12.
- ¹³J. D. Jackson, *Classical Electrodynamics*, 2nd ed. (Wiley, New York, 1975).
- ¹⁴C. A. MacDonald, W. M. Gibson, and W. W. Pepler, "X-ray optics for better diagnostic imaging," *Technol. Cancer Res. Treat.* **2**, 111–117 (2002).
- ¹⁵C. A. MacDonald, N. Mail, D. Li, M. Roy, and F. Sugiro, *Laser-Generated and Other Laboratory X-ray and EUV Sources, Optics, and Applications*, edited by George A. Kyrala, Jean-Claude J. Gauthier, Carolyn A. MacDonald, and Ali M. Khounsary, SPIE 5196, pp. 405–411, 2003.
- ¹⁶E. Gullikson, "Filter transmission," X-ray Interaction with Matter. CXRO: Berkeley, 2002. Website: http://www-cxro.lbl.gov/optical_constants/filter2.html
- ¹⁷J. H. Hubbell and S. M. Seltzer, Tables of X-ray Mass Attenuation Coefficients and Mass Energy-Absorption Coefficients. U. S. Secretary of Commerce: Gaithersburg, 1996. Website: <http://physics.nist.gov/PhysRefData/XrayMassCoef/tab3.html>
- ¹⁸L. I. Mirkin and Lev Iosifovich, *Handbook of X-ray Analysis of Polycrystalline Materials* (Consultants Bureau, New York, 1964).
- ¹⁹A. G. Michette and C. J. Buckley, *X-ray Science and Technology* (Institute of Physics Publishing, Bristol, 1993).
- ²⁰Danhong Li, F. R. Sugiro, and C. A. MacDonald, "Source-optic-crystal optimization for compact monochromatic imaging," edited by Carolyn A. MacDonald, Albert T. Macrander, Tetsuya Ishikawa, Christian Morawe, and James L. Wood, SPIE 5537, 2004 (to be published).
- ²¹D. G. Kruger, C. C. Abreu, E. G. Hendee, A. Kocharian, W. W. Pepler, C. A. Mistretta, and C. A. MacDonald, "Imaging characteristics of x-ray capillary optics in mammography," *Med. Phys.* **2**, 187–196 (1996).
- ²²*CRC Handbook of Physics and Chemistry*, 85th ed., edited by David Lide (CRC, 2005).
- ²³G. Holzer *et al.*, "Flat and spherically bent muscovite (Mica) crystals for x-ray spectroscopy," *Phys. Scr.* **57**, 301–309 (1998).
- ²⁴B. D. Cullity, *Elements of X-ray Diffraction*, 2nd ed. (Addison-Wesley, Reading, 1978).